Check for updates

Research Article

Nanosized Transferosome-Based Intranasal *In Situ* Gel for Brain Targeting of Resveratrol: Formulation, Optimization, *In Vitro* Evaluation, and *In Vivo* Pharmacokinetic Study

Heba F. Salem,[1,3] **Rasha M. Kharshoum,**[1] **Heba A. Abou-Taleb,**[2] and **Demiana M. Naguib**[2]

Abstract. Resveratrol (RES) is a potent antioxidant used for the management of several central nervous system diseases. RES bioavailability is less than 1 owing to its low solubility and extensive intestinal and hepatic metabolism. The aim of the study was to enhance RES bioavailability through developing intranasal transferosomal mucoadhesive gel. Reverse evaporation–vortexing sonication method was employed to prepare RES-loaded transferosomes. Transferosomes were developed *via* 3^4 definitive screening design, using soya lecithin, permeation enhancers, and surfactants. The optimized formula displayed spherical shape with vesicle size of 83.79 ± 2.54 nm and entrapment efficiency (EE%) of $72.58 \pm 4.51\%$. Mucoadhesive gels were prepared and evaluated, then optimized RES transferosomes were incorporated into the selected gel and characterized using FTIR spectroscopy, *in vitro* release, and *ex vivo* permeation study. Histopathological examination of nasal mucosa and *in vivo* pharmacokinetic study were conducted. *In vitro* drug release from transferosomal gel was $65.87 \pm 2.12\%$ and *ex vivo* permeation was $75.95 \pm 3.19\%$. Histopathological study confirmed the safety of the optimized formula. The C_{max} of RES in the optimized RES trans-gel was 2.15 times higher than the oral RES suspension and $\text{AUC}_{(0-\infty)}$ increased by 22.5 times. The optimized RES trans-gel developed intranasal safety and bioavailability enhancement through passing hepatic and intestinal metabolism.

KEY WORDS: transferosomes; resveratrol; intranasal mucoadhesive gel; permeation enhancer.

INTRODUCTION

Resveratrol (RES) is a plant-derived polyphenol compound isolated from red grapes, peanuts, and mulberries (1). It has attracted remarkable attention due to its wide therapeutic benefits treating and preventing numerous diseases including cardiovascular diseases, neurodegenerative diseases, diabetes mellitus, and cancer; it possesses antioxidant and anti-inflammatory effects and thus plays a critical role in the therapeutic effect (2,3). RES possesses antimicrobial effects against herpes simplex virus (4); furthermore, there is evidence that it is useful in the treatment of Alzheimer's disease (5,6). Despite the wide therapeutic benefits of RES, its application remains very limited due to the following limitations: photochemical degradation; poor aqueous solubility (~ 3 mg/100 ml) (7); short biological half-life, which is a consequence of extensive intestinal and hepatic

metabolism; and accordingly the oral bioavailability (less than 1%) (7,8).

A proper drug delivery system is required to overcome the mentioned limitations. Recently, novel formulation approaches have occupie an encouraging new area for RES's delivery providing numerous advantages, such as polymeric nanoparticles (9), complexation with cyclodextrin (10), micelles (11), and liposomes (12), chitosan microparticles (13), polymeric lipid-core nanocapsules (14), solid lipid nanoparticles (15), emulsion–liposome blends (16), transferosomes, ethosomes, and transethosomes (17). Nasal drug delivery has showed great interest recently as a promising route since it provides numerous advantages over oral or parenteral administration (18,19). Intranasal route is non-invasive and painless besides the high vascularization through the epithelium increasing drug absorption (20,21); also, nasal route avoids the hepatic and intestinal metabolism and enables brain drug delivery directly *via* the olfactory and trigeminal nerves and indirectly *via* the vascular pathway (19,22). Studies have been recently reported that intranasal drug delivery can be effective for the management of several central nervous system diseases such as Alzheimer's diseases (23), Parkinson's disease (24), brain tumors, sleep disorders (25), and schizophrenia (26). However, short nasal residence

[1] Department of Pharmaceutics, Faculty of Pharmacy, Beni-Suef University, El Shahed Shehata Ahmed Hegazy St, Beni-Suef, Egypt.
[2] Department of Pharmaceutics, Faculty of Pharmacy, Nahda University (NUB), Beni-Suef, Egypt.
[3] To whom correspondence should be addressed. hebasalem3313@gmail.com)

time owing to the rapid mucociliary clearance, low mucosal permeability of the hydrophilic drugs, and the small surface of the nasal cavity are assumed to be the major limitations for the nasal drug delivery (27). Accordingly, the majority of recent studies oriented toward the development of mucoadhesive nasal formulations also the use permeation enhancers to enhance the nasal absorption and increase the nasal residence time (28).

Transferosomes are ultradeformable and very flexible vesicles composed mainly of phospholipids and a permeation enhancer (PE), first introduced by Cevc and Blume in 1992 (29). They have the privilege of the deformability over liposomes due to the presence of PE that soften the lipid bilayers. Deformability enables them to change their shape and easily squeeze between cells enhancing the permeation (30,31). The aim of the present study is to enhance RES bioavailability and to accomplish direct nose to brain targeting through an optimum transferosomal formulation. Reverse evaporation–vortexing sonication method was employed to prepare RES-loaded transferosomes using 3^4 definitive screening design. Transferosomes were characterized for globule size, *in vitro* release, and encapsulation efficiency, then they were optimized using Design Expert® software. The optimum formula was developed and characterized for vesicle size, encapsulation efficiency, *in vitro* release, stability study, and FTIR analysis. Mucoadhesive gels were prepared and evaluated, then the optimum transferosomes were incorporated into the selected gel and subjected to *in vitro* release, *ex vivo* permeation, histopathological examination for nasal mucosa tolerability, and finally were applied to *in vivo* pharmacokinetics study.

MATERIALS AND METHODS

Materials

Resveratrol was a kind gift from Eipico, Egypt. Tween 80 (polyoxyethylene sorbitan monooleate, HLB = 15), Cremophor RH 40 (polyoxyethylene 40 hydrogenated castor oil, HLB, 14–16), and oleic acid (octadecenoic acid) were purchased from Lab Chemicals Trading Co., Egypt. Transcutol (diethylene glycol monoethyl ether) was purchased from Sigma Chemicals, St. Louis, USA. Sodium deoxycholate, polyoxyethylene sorbitan monolaurate (Tween 20), and dialysis bags with a molecular weight cut-off of 12,000 kDa were purchased from Sigma-Aldrich (St. Louis, MO). L-α-phosphatidyl-choline (soya lecithin), Carbopol 934, and Poloxamer 407 were a kind gift from Eipico. Methanol and acetonitrile (HPLC grade) were purchased from Romil, London, UK. Triethanolamine was purchased from Adwic Co., Cairo, Egypt.

Methods

Formulation of Resveratrol-Loaded Transferosome

RES-loaded transferosomes were formulated using reverse evaporation with vortexing–sonication method with minor modifications determined according to preliminary studies (32,33). Briefly, RES (10 mg) along with surfactant and soya lecithin were dissolved in (2:1) chloroform/methanol and vortex mixed for 10 min. The resulting mixture was allowed to form a dried thin film at room temperature for 24 h in a desiccator. The obtained film was hydrated with 10 ml of simulated nasal fluid (SNF, pH 5.5) (34) containing permeation enhancer (PE) except for oleic acid, which was added with soya lecithin; the obtained vesicles were allowed to swell for 2 h at room temperature then vortexed for 20 min. The obtained large vesicles were sonicated by a probe sonicator for 20 min, then extruded through a 0.2-μm Sartorius membrane filter (GMBH, Germany) three times to reduce their size further. The vesicles were separated using a cooling centrifuge (Hettich Zentrifugen, Germany) for 3 h at 20,000 rpm at 4°C, then washed with simulated nasal fluid. The prepared transferosomes were stored at 4°C in tightly closed amber tubes for further studies.

Experimental Design and Optimization of Transferosomal Formulation

A four-factor, three-level definitive screening design (34) (Table I) was employed for optimization procedure *via* response surface experimental study. Ratio of soya lecithin (PC) to permeation enhancer (PE) (X1), ratio of (PC) and (PE) to surfactants (X2), type of surfactants (Tween 80, sodium deoxycholate, Cremophor RH 40) (X3), and type of PE (transcutol, oleic acid, ethanol) (X4) were selected as four prime selected independent variables, which were varied at three levels, low (− 1), intermediate (0), and high level (+1). These levels were determined according to preliminary studies. Consequently, vesicle size (Y1), percentage of *in vitro* release (Y2), and entrapment efficiency (EE%) (Y3) were used as dependent variables for the optimization method. Fourteen transferosomal formulations were prepared using Design-Expert® software (version 10.0.0.3; Manugistics Inc., Rockville, USA), as shown in Table II.

The adjusted and predicted coefficient of determination (R^2) and CV% values were utilized to assess the suitability of the used model to investigated data. Besides, the statistical significance was assessed through F test involved in the lack of fitness and the analysis of variance (ANOVA) at P value is less than 0.05. Adequate precision is used to measure the signal-to-noise ratio to ensure that the model can be utilized to navigate the design space.

Characterization of RES-Loaded Transferosomes

Vesicle Size, PDI, and Electric Potential Analysis. The vesicles' mean diameter, size distribution curve, and electric potential were determined through dynamic light scattering using Malvern Zetasizer (ver.7.11, serial number MAL1121994). The prepared transferosomal formulations were diluted 100 times and the measurements were repeated in triplicate, and the results are shown in Table II.

Determination of RES Encapsulation Efficiency (%EE). The encapsulation capacity of transferosomes was determined as follows: RES-loaded transferosomes were separated using centrifugation for 4 h at 4°C and 20,000 rpm. The obtained supernatant was diluted with SNF, pH 5.5, and analyzed using a UV spectrophotometer (Shimadzu, Japan) for the drug content at 306 nm. Percentage

Table I. Four-Factor, Three-Level Definitive Screening Design (3^4) Through Response Surface Experimental Study

Factors	Levels		
	− 1	0	1
Ratio of PC/PE (w/w)	7:3	8:2	9:1
Ratio of PC + PE/surfactant (w/w)	2:1	3:1	4:1
Type of surfactant	Tween 80	Na-deoxycholate	Cremophor
Type of PE	Transcutol	Oleic	Ethanol

Table III. Composition of the Developed Mucoadhesive Gels

Formula	Poloxamer % w/v	Carbopol % w/v
1	16	0.6
2	16	0.4
3	16	0.2
4	18	0.6
5	18	0.4
6	18	0.2
7	20	0.6
8	20	0.4
9	20	0.2

of the encapsulated RES (%EE) was calculated according to the following equation (Eq. 1) (35, 36).

Encapsulation efficiency(%EE)

$$= \frac{\text{amount encapsulated (total amount−free amount)} \times 100}{\text{total amount}}$$

(1)

In Vitro RES Release and Kinetics Analysis of the Release Data. RES *in vitro* release from the prepared transferosomes was conducted by dialysis membrane technique (37,38). Loaded transferosomal suspension equivalent to 10 mg RES was positioned in the donor compartment using an open-sided tube that was enveloped from one side with dialysis cellophane membrane (MWt of 12,000 kDa) and the other side was reinforced in a paddle-type, USP dissolution apparatus; the paddle was stirred at 100 rpm. Fifty milliliters of SNF (pH 5.5) was used as receptor medium, the temperature of the medium was well maintained at 37 ± 0 .5°C, and to maintain a sink condition, 20% of propylene glycol was added (30). Aliquots of 1 ml were withdrawn at different time intervals (0.5, 1, 2, 3, 4, 5, 6, 8, and 12 h) and substituted by equivalent amounts of fresh medium; all the experiments were repeated three times. The withdrawn samples were analyzed spectrophotometrically at 306 nm. RES percentage of *in vitro* release was calculated by dividing the initial amount of the encapsulated RES by the amount of RES released at time *t* multiplied by 100 (39). RES percentage of *in vitro* release from loaded transferosomes were

compared with that of 10 mg of the free drug suspension. The release kinetics of RES was determined by fitting the data obtained from the release studies to the different kinetic models. The most appropriate model to describe RES release order was selected according to the highest value of correlation coefficient (R^2) (37). Based on the characterization of the prepared transferosomal formulae, the optimized formula was determined.

Formulation and Characterization of the Optimized RES Transferosomal Formulation

Formulation of the Optimized RES-Loaded Transferosomes. The optimized RES-loaded transferosome was selected utilizing response surface experimental study based on minimum particle size, maximum *in vitro* released RES, and maximum EE%. Subsequently, the optimized loaded transferosomes were formulated using reverse evaporation with vortexing–sonication technique as prescribed previously and applied to characterization procedure.

Characterization of the Optimized RES Transferosomes. The optimized loaded RES transferosomes were prepared and analyzed for vesicle size, PDI, EE%, and % of RES released as prescribed previously. Also, Fourier-transform infrared spectroscopy (FTIR) was analyzed. The IR spectra using dried potassium bromide for the pure RES and the physical mixture of the

Table II. Observed Responses in the Design for RES in Different Transferosomal Formulations' Definitive Screening Design

Sample number	X1	X2	X3	X4	Size (nm) (Y1)	PDI	Zeta potential	EE% (Y3)
1	− 1	− 1	1	0	84.25 ± 3.2	0.271	− 17.6	59.53 ± 2.21
2	− 1	0	1	− 1	97.49 ± 2.4	0.259	− 24.2	48.84 ± 2.28
3	1	0	− 1	1	195.3 ± 4.7	0.185	− 18.9	72.73 ± 1.40
4	1	− 1	1	1	88.81 ± 2.2	0.346	− 17.5	65.78 ± 3.39
5	− 1	1	0	1	83.61 ± 1.7	0.285	− 29.9	57.63 ± 2.63
6	− 1	− 1	− 1	1	102.40 ± 3.6	0.289	− 12.5	38.32 ± 2.48
7	1	1	1	− 1	168.5 ± 5.2	0.247	− 28.7	80.30 ± 2.56
8	− 1	1	− 1	− 1	191.2 ± 6.5	0.177	− 29.0	53.10 ± 2.37
9	1	1	− 1	0	189.5 ± 4.8	0.189	− 35.5	94.85 ± 1.85
10	0	1	1	1	184.4 ± 6.3	0.136	− 33.8	68.75 ± 3.00
11	0	0	0	0	95.35 ± 3.5	0.203	− 29.0	81.80 ± 1.62
12	1	− 1	0	− 1	94. 93 ± 3.6	0.194	− 24.0	74.35 ± 2.93
13	0	− 1	− 1	− 1	125.6 ± 2.7	0.312	− 18.0	53.14 ± 1.91
14	0	0	0	0	94.97 ± 2.8	0.286	− 23.0	82.33 ± 2.60

Table IV. Data of Regression Analysis and Analysis of Variance of All Dependent Variables

Source	Size (nm)		Release %		EE%	
	F value	P value	F value	P value	F value	P value
Model	84.26	< 0.0001	46.83	< 0.0001	167.03	< 0.0001
A-PC:EA	147.42	< 0.0001	*196.02*	*< 0.0001*	*491.06*	*< 0.0001*
B-PC + EA:S	17.05	0.0003	*125.83*	*< 0.0001*	*204.55*	*< 0.0001*
C-S	439.52	< 0.0001	*6.03*	*0.0199*	*42.64*	*< 0.0001*
D-EA	12.86	0.0012	*0.85*	***0.3631***	*43.37*	*< 0.0001*
AB	39.00	< 0.0001	*37.57*	*< 0.0001*	*93.28*	*< 0.0001*
AD	149.61	< 0.0001	*8.32*	*0.0071*	*11.45*	*0.0020*
BC	44.15	< 0.0001	*18.34*	*0.0002*	*260.47*	*< 0.0001*
BD	92.14	< 0.0001	–	–	–	–
R^2	0.9574		0.9136		0.9742	
Adjusted R^2	0.9460		0.8941		0.9683	
Predicted R^2	0.9198		0.8396		0.9508	
Adequate precision	36.180		30.302		47.375	
CV %	0.9198		4.45		3.56	
Lack of fit (P value)	0.2426		0.2734		0.3861	
Ln (vesicle size) = + 4.80 + 0.12A + 0.065B − 0.18C + 0.049D + 0.12AB + 0.32 AC + 0.12 AD + 0.21BD					**3**	
In vitro release = + 64.92 − 8.47A − 10.39B − 1.37C + 0.72D − 5.17AB − 2.55 AD + 3.03 BC					**4**	
Entrapment = + 65.78 + 10.98A + 10.85B + 2.99C + 4.23D + 6.67AB − 2.45 AD − 9.34 BC					**5**	

optimized transferosomal formula were compared with that of each separate component, so as to study the interaction between them; the spectra were recorded over the range of 400 to 4000 cm^{-1} (37). The morphology of the optimized loaded transferosomal formula was determined by manipulating transmission electron microscopy (TEM) (JEOL JEM-1400, Tokyo, Japan). Carbon–copper grid was covered with a drop of freshly prepared formula and left to dry to allow the vesicles to stick to the carbon substrate. The vesicles were
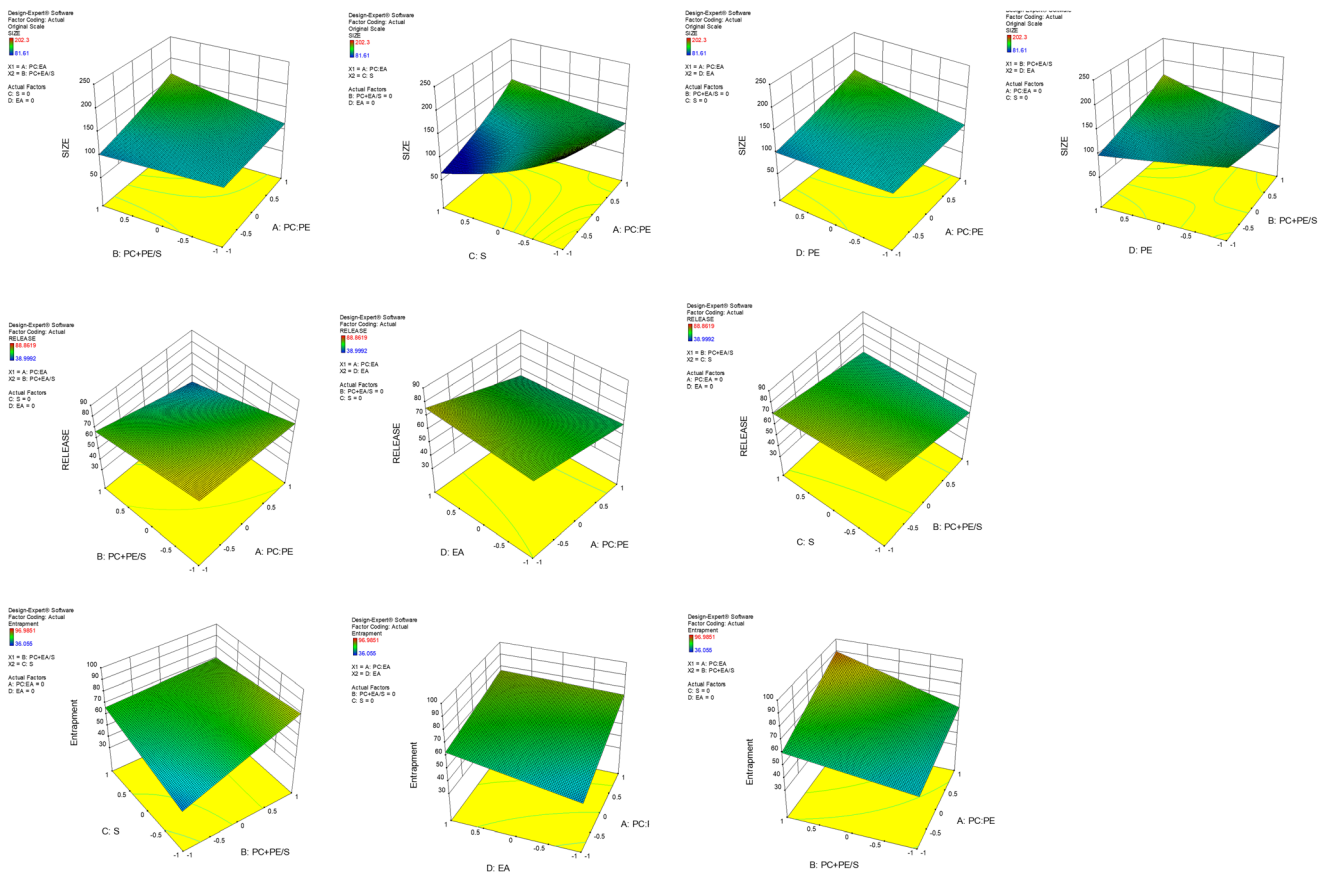
Fig. 1. The impact of the independent variables on the responses characterized by 3D-response surface graphs
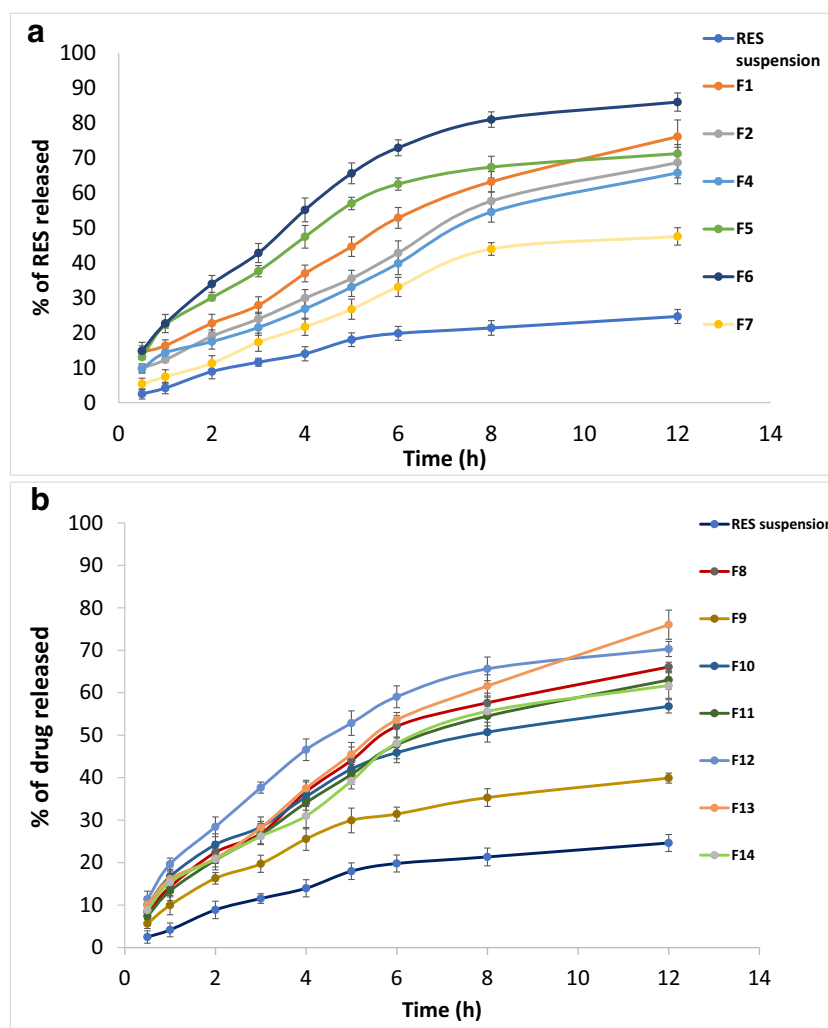
Fig. 2. *In vitro* release profiles of RES from the prepared transferosomes: **a** F1–F6, **b** F7–F14

stained using phospho-tungstic acid dye and allowed to dry, then the stained vesicles were visualized using TEM through an accelerating voltage of 80 kV (40,41).

Stability Study. Stability testing of the optimized loaded RES transferosomes was determined through storing the optimized formula (5 mg RES/5 ml) in tightly closed amber glass vials in the refrigerator at 4°C and at room temperature of 25°C up to 3 months. Samples were withdrawn and characterized by the vesicle's diameter and EE% (42). The study was repeated in three replicates. In order to inspect the significance of the results, Tukey *post hoc*, one-way ANOVA was utilized.

Preparation of Mucoadhesive Nasal Gel

Cold method was utilized to prepare mucoadhesive nasal gels (43). Plain transferosomes were dispersed in cold SNF (4°C), Carbopol 934 was added portion wise, and the mixture was stirred subsequently; Poloxamer 407 was added with continuous stirring until a clear solution was obtained, then two drops of triethanolamine were lastly added (44). Nine

mucoadhesive nasal gel formulations were prepared and kept in refrigerator (4–8°C) for additional characterization to select the most appropriate formulation for RES transferosome loading, and the composition of these formulations is shown in Table III.

Characterization of Mucoadhesive Nasal Gel

Gelation Temperature. Visual inspection method (45) was employed to determine gelation temperature of the prepared gels. Briefly, 5 ml of each nasal gel (of the same temperature) was placed in a 20-ml beaker comprising a magnetic bar with a thermometer immersed in it, and the beaker was placed in a hot plate magnetic stirrer. The hot plate temperature was raised at a rate of 10°C/min and the stirring was fixed at 30 rpm. Gelation temperature was recorded when the magnetic bar stopped stirring, and the test was triplicated.

Gelation Time. Nasal mucoadhesive gel (5 ml) was placed in a 20-ml beaker containing a magnetic bar and the beaker was placed over a hot plate magnetic stirrer; its temperature was maintained at 34°C and the stirring was fixed at 30 rpm. Gelation time was recorded when the magnetic bar stopped stirring and the test was triplicated (18).
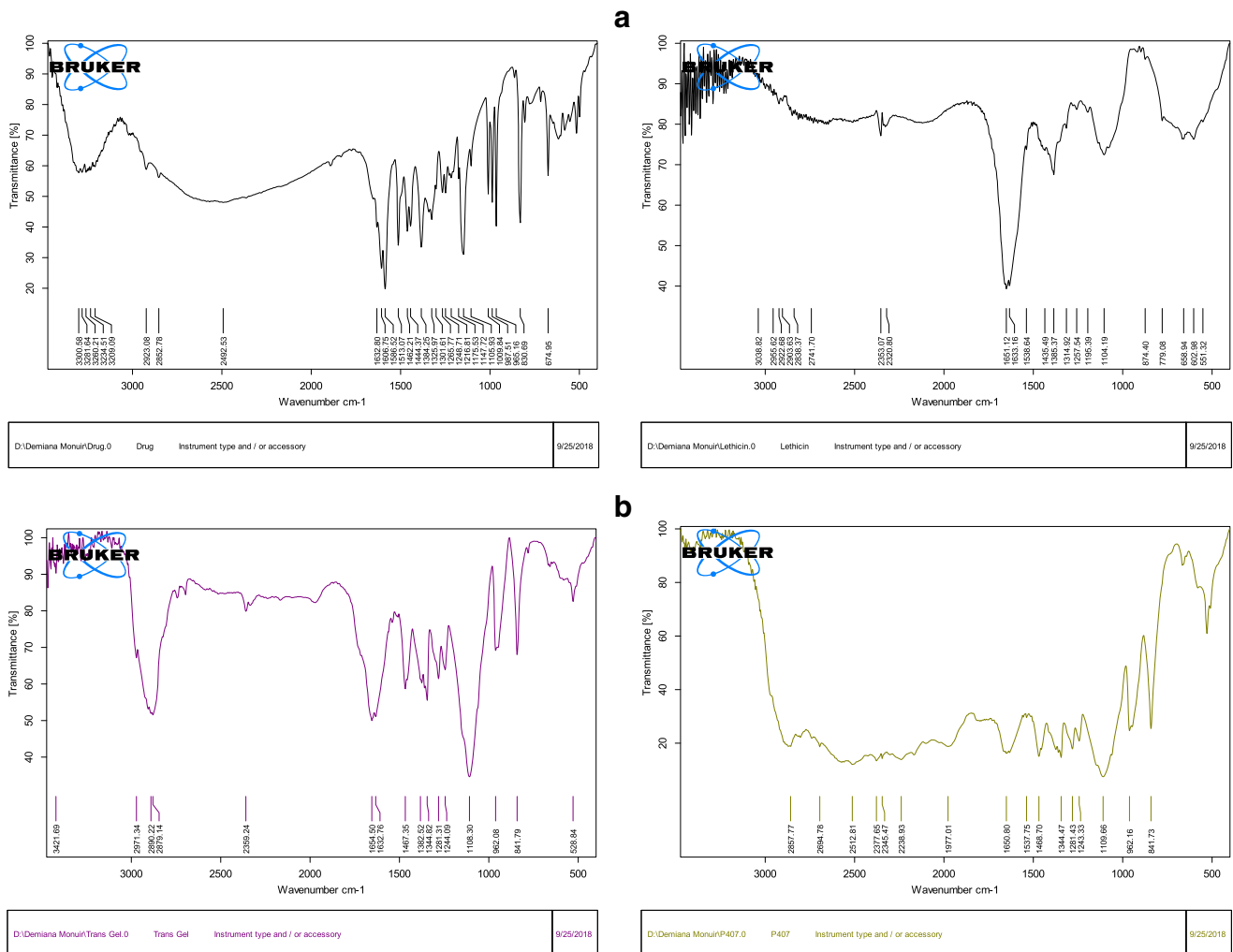
Fig. 3. The Fourier-transform infrared (FTIR) spectra of pure RES, the physical mixture of the optimized RES-loaded transferosome, the physical mixture of the selected mucoadhesive gel, Carbopol 934, poloxamer 407 soya lecithin, Cremophor RH 40, and ethanol

Mucoadhesive Strength. Mucoadhesive strength is equivalent to the force needed to separate the mucoadhesive gel from the nasal mucosa (43). Intact nasal mucosal membrane was isolated from nasal tissue of sheep, obtained from a local slaughter house, within 1 h after slaughtering the animal. The isolated nasal mucosal membrane was cleaned after with 0.9% *w/v* saline. Portions of nasal mucosa were approximately 2.5×1 cm²; each of them was tied to a glass slide with cyanoacrylate glue and fixed to the lower part of a pan balance and another glass slide was connected to the balance in an inverted position allowing the two portions of nasal mucosa to face each other. One gram of mucoadhesive gel was placed between the tissues and held in contact for 5 min then dummy powder was added gradually into the other pan until the nasal mucosa had detached (43). The mucoadhesive force was calculated using the following equation (Eq. 2) (46):

$$\text{Mucoadhesive strength}\left(\text{dyne/cm}^2\right) = \frac{M \times G \times 100}{A} \qquad (2)$$

where *M* is the weight in grams required for detachment, *G* is the acceleration due to gravity, and *A* is the area of nasal mucosa exposed (cm²).

Gel Strength. Twenty-five grams of the mucoadhesive gel was placed in a 50-ml measuring cylinder and gelled at 34°C. Subsequently, weight of 17 g was positioned onto the gel surface and the time needed by this weight to deep penetrate 5 cm into the mucoadhesive gel was determined as gel strength (47).

Statistical Analysis. SPSS 16.0 software was utilized for statistical data analysis applying one-way ANOVA and Tukey *post hoc* test to evaluate the statistical significance at $P < 0.05$.

Preparation and Characterization of RES-Loaded Transferosomal Nasal Gel (RES-TRS Gel)

The optimized RES-TRS gel was eventually prepared, and briefly Poloxamer 407 (18%) and Carbopol 934 (0.4%) were added to the optimized RES transferosomal dispersion applying the same procedure used for blank gel preparation. The prepared RES-TRS gel was subjected to the following characterization procedure.

The optimized RES-TRS gel was characterized *via* FTIR, and the IR spectra using dried potassium bromide for the physical mixture of the optimized RES-TRS gel were compared with that of each separate component and with the spectra of the pure RES.
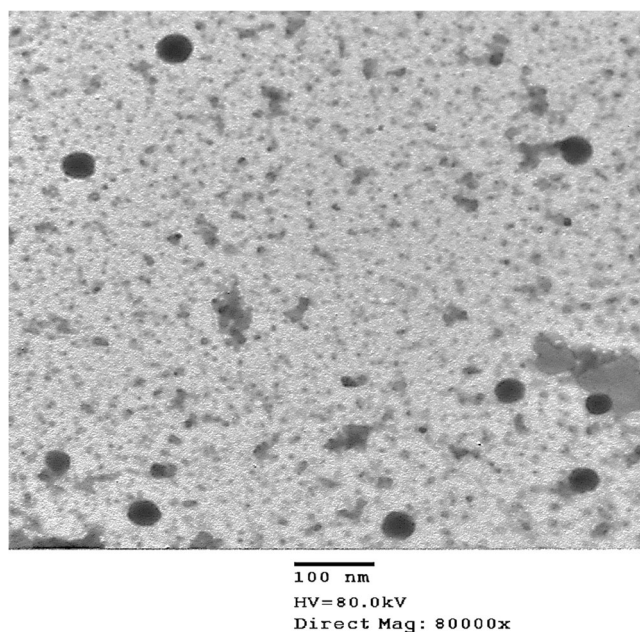
Fig. 4. Photomicrograph of optimized RES-loaded transferosome using TEM

Also, RES *in vitro* release and the release kinetics were determined as prescribed previously. Also, the optimized RES-TRS gel was tested for permeation behavior against RES suspension gel through sheep nasal mucosa instead of

the dialysis cellophane membrane, used formerly throughout the dialysis method utilized during *in vitro* release studies with the same test conditions. The percentage of drug permeated was calculated up to 12 h and the permeation parameters including permeation flux and permeation coefficient were calculated according to the method prescribed by Al Shuwaili et al. (33). Sheep nasal mucosa was obtained from a local slaughter house. After mucosa separation, it was washed using SNF and used freshly (48).

### Histopathology for Nasal Mucosal Toxicity and Tolerability

Five Wistar albino rats weighing 210 to 240 g received once-daily nasal dose of 50 µl of optimized RES-TRS gel for 7 days. The nasal septum of the sacrificed rats was carefully separated from the bone with the epithelial cell membrane. The nasal septum was fixed using 10% formalin, decalcified, and dehydrated using ethanol. Tissue blocks were prepared using paraffin beeswax and dried in a hot-air oven, then sliced using a microtome at 5 µm. The obtained slices were then deparaffinized and stained using hematoxylin and eosin stains and examined using a light microscope against untreated tissues (49).

In Vivo Pharmacokinetic Study

Two groups of male Wistar albino rats ($n = 6$), weighing 250–280 g, were used in the pharmacokinetic study. Group 1 received oral RES suspension, while group 2 received the
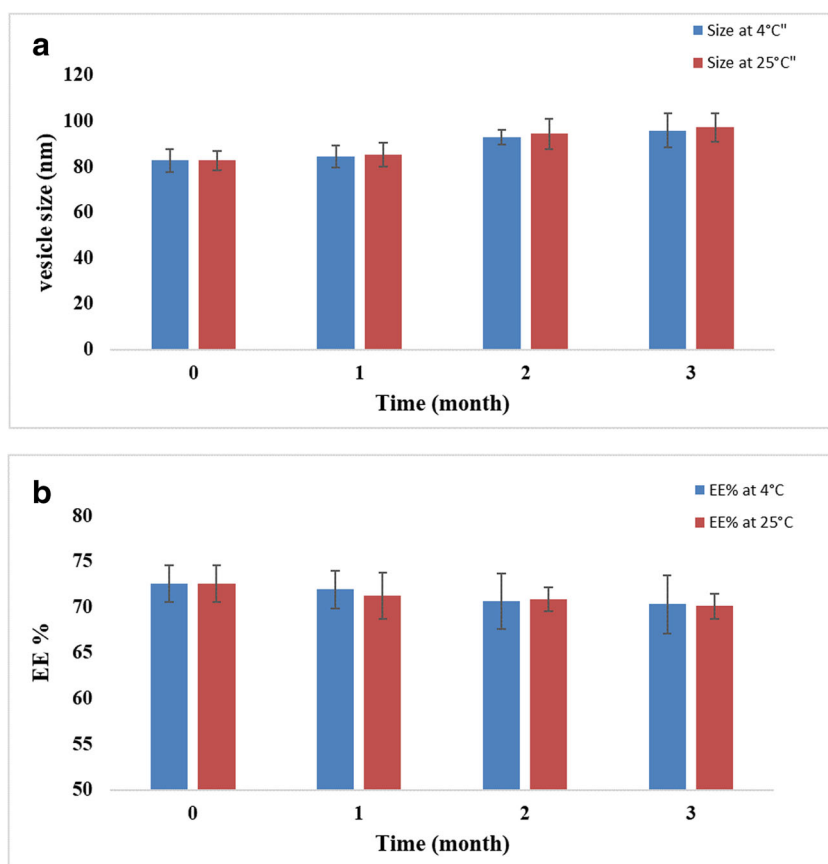
Fig. 5. Effect of storage on the vesicle size and EE% of the optimized loaded transferosomes at 4 and 25°C
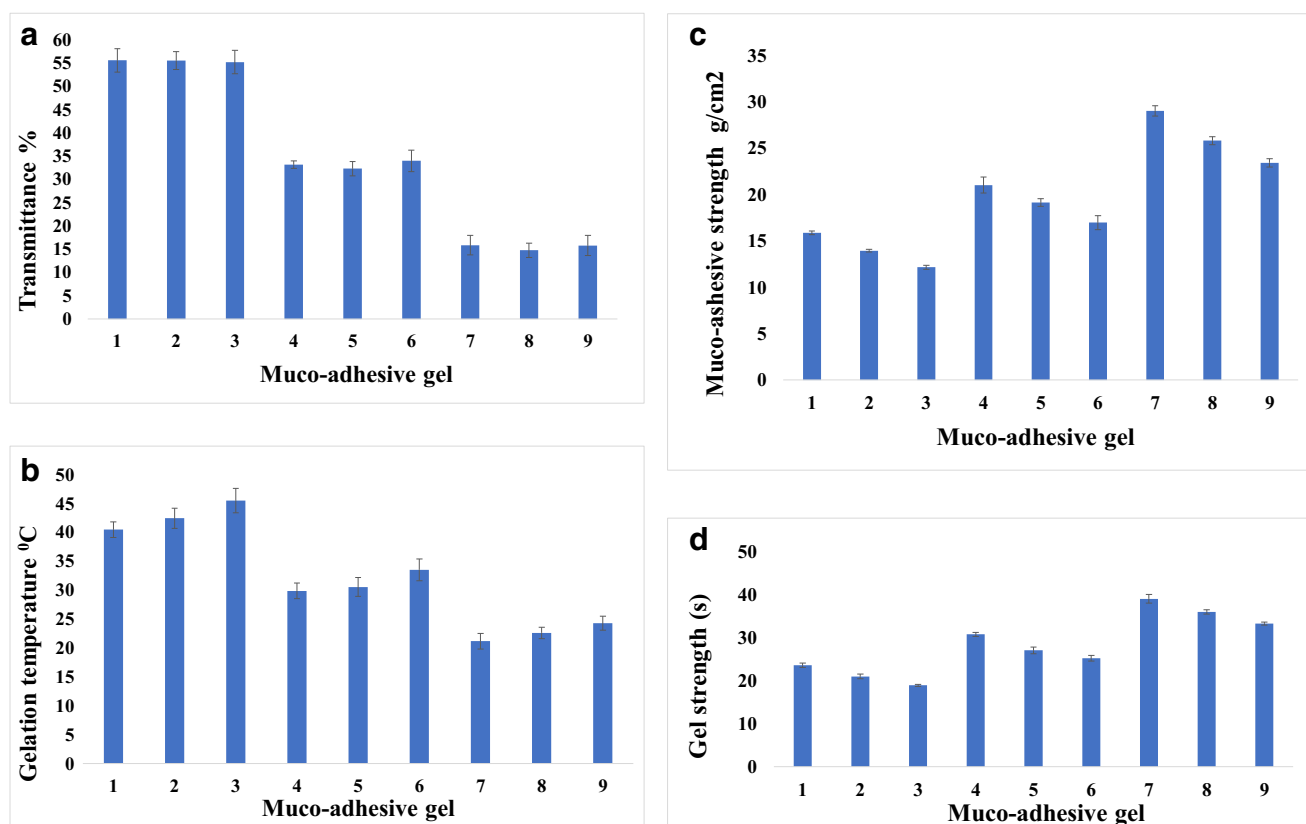
Fig. 6. Characterization of mucoadhesive nasal gels; **a** gelation time, **b** gelation temp, **c** mucoadhesion strength, and **d** gel strength

optimized intranasal RES-TRS gel at a dose of 20 μg/kg (50). Aliquots of the blood samples were withdrawn under minor di-ethyl ether anesthesia, from retro-orbital plexus at a range of time intervals (0.1, 0.5, 1.5, 2, 4, 8, 16, 24 h), and placed in the heparinized tubes (51). The *in vivo* study protocol was approved by the ethical committee of Beni-Suef University.

Blood samples were centrifuged at 20°C, 15,000 rpm, then to separate the plasma proteins, 50 μl of acetonitrile was added followed by vortex mixing and centrifugation. The harvested plasma samples were analyzed for RES content at 306 nm using HPLC method as prescribed by Singh et al. (52). The pharmacokinetic parameters (C_{max}, T_{max}, AUC, $t_{1/2}$, and MRT) were computed by choosing PK Solver

software. The SPSS 16.0 software (SPSS Inc., Chicago, IL) was utilized for statistical data analysis.

RESULTS AND DISCUSSION

Optimization of Transferosomal Formulation and Experimental Model Estimation

So as to optimize the RES-loaded transferosome, relationships among the studied independent variables were A (ratio of PC to PE), B (ratio of PC and PE to surfactants), C (type of surfactant), and D (type of PE), at three levels (− 1, 0, + 1). The examined dependent variables Y1 (vesicle size), Y2 (*in vitro* release), and Y3 (entrapment efficiency)
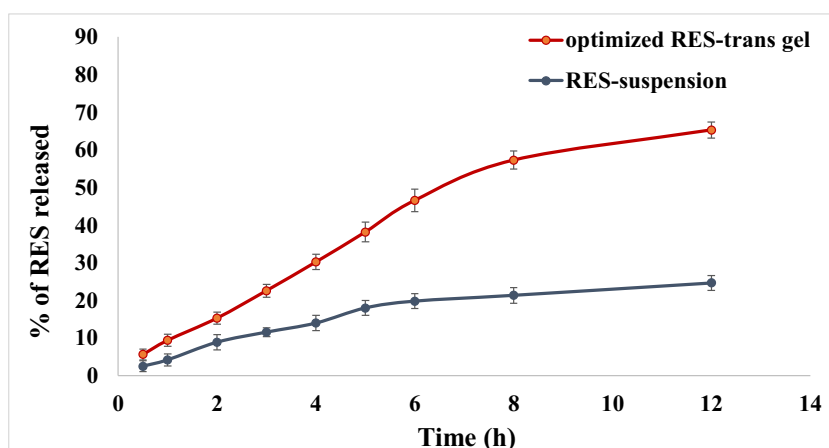
Fig. 7. *In vitro* percentage of release of the optimized RES-trans gel and RES suspension

Table V. The Correlation Coefficients for *In Vitro* Release and *Ex Vivo* Permeation

	Curve fitting model (R^2)				
	Zero order	First order	Huguchi model	Hixson–Crowell	Korsmeyer–Peppas
In vitro release	0.9974	0.9836	0.9607	0.9912	0.9334
Ex vivo permeation	0.9952	0.9784	0.9592	0.9875	0.9281

were assessed by definitive screening design *via* Design Expert® software. R2FI was found to be the superlative model obtained for all three dependent variables, and all models were significant at *P* value of 0.05 (Table IV). Most the individual models in Table IV were significant (*P* < 0.05), excluding a few terms (showed in bold). Mathematical relationships for the examined dependent variables are represented in the following equations (Eq. 3–5), shown in Table IV. The effect of the factor on the response was termed synergistic with the positive coefficient and antagonistic effect with negative coefficient (53). The adjusted coefficient of determination (adjusted R^2) and the predicted one (predicted R^2) were in a reasonable agreement through all responses. The applied model can be utilized to navigate the design space as the adequate precision that measures the signal-to-noise ratio is greater than 4 (Table IV) (40).

**The Effect of Formulation Variables on the Tested Response**

From the obtained equations (Table IV), it is obvious that the intercept has positive impacts for all three responses. The impact of the independent variables on the responses are characterized by 3D-response surface graphs as represented in Fig. 1.

The entrapment efficiency of the investigated transferosomes ranged from 38.32 ± 2.48% to 94.85 ± 1.85% as shown in Table II. This high RES entrapment might be a result of the water insolubility due to hydrophobicity of RES (log *P* = 3.1) (54). The results of the ANOVA test indicated that all the four factors including X1 = ratio of PC to PE, X2 = ratio of PC and PE to surfactants, X3 = type of surfactants, and X4 = type of PE had significant impact on the entrapment at *P* < 0.05. A synergistic significant impact was noticed for the tested variables (A, B, C, and D) except for AD and BC, which showed a significant antagonist

interaction. With respect to the type of PE and surfactant, it was clear that the entrapment decreased upon increasing PE and surfactant ratios. The increased concentrations of surfactant and PE lead to increased elasticity and weakening of the lipid bilayer and that might cause aperture formation in the lipid bilayer (33,55). Also, increased PE concentration may lead to micelle formation, leading to a decrease in entrapment (56). The vesicles that contained oleic acid as PE showed a significantly higher percentage of entrapment than any other PE used, and changing the concentration of oleic acid showed a significant effect on the %EE; the results are in contrast with (40) and go along with (57).

Transferosomal vesicle size ranged from 83 to 195 nm (Table II). A synergistic significant impact on the vesicle size was noticed for all tested variables (A, B, D) except for C which showed an antagonist impact and a synergistic interaction that was exhibited for AB, AC, AD, and BD. The increase in the ratios of PE and surfactants to PC results in a significant reduction in the vesicle size which could be attributed to the dropped interfacial tension using a high surfactant concentration and to the steric stabilization and electrostatic repulsion which was caused by the prepared transferosomal negative charge (58) (Table II). These results are in accordance with Shamma and Elsayed (40) for using oleic acid while the results are in contrast with them for using ethanol. The least size was obtained for transcutol followed by oleic acid then ethanol as PE; for the surfactant, Cremophor RH 40 followed by sodium deoxycholate then Tween 20; that order goes along with (30).

In vitro percentage of release ranged from 39.91 ± 1.18% to 85.90 ± 2.61% (Fig. 2). A synergistic significant impact on the *in vitro* release was observed for the following tested variable (D) while A, B, and C showed an antagonist impact; a synergistic interaction was observed for BC, while an antagonist interaction was observed for AB and AD. Results
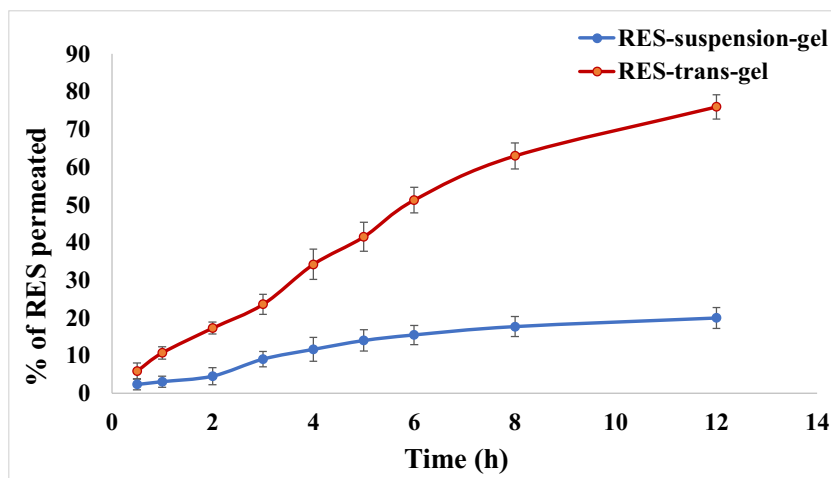
Fig. 8. *Ex vivo* percentage of permeation of the optimized RES-trans gel and RES suspension

Table VI. *Ex Vivo* Permeation Parameters of RES-Transferosome *Versus* Pure RES Suspension

Formulation	Flux (Jss) (μg cm^{-2} h^{-1})	Permeation coefficient (cm/h)
RES suspension	0.070969996	0.000007
RES-transferosome	0.321486699	0.000032

indicated that RES *in vitro* release was principally affected by the PC ratio to PE and surfactant, the highest PE and surfactant ratios, and the maximum RES release. The higher *in vitro* release percentage is attributed to the dual effect of PE and surfactant, as they increase the partitioning of RES from transferosomes through improving vesicular bilayer fluidity and enhancing RES solubility (59). RES release outcomes were fitted to different release kinetic models so as to estimate release kinetics. According to linear regression analysis, the most fitting model that explains the release kinetics is zero order, while F9 obeys Huguchi model; they possess a controlled drug release rate, except for F10 and F12 in which their release kinetics obeys first-order kinetics.

The Optimization and Characterization of the Optimized RES Transferosomes

The effect of tested variables on the established responses has been studied as previously mentioned. The goal of the numerical optimization is to find a point that maximizes the desirability function; desirability ranges from zero outside of the limits to one at the goal. The optimization criteria were based on minimizing transferosome size and maximizing the *in vitro* release and encapsulation entrapment to obtain the optimized transferosome that have the highest desirability (nearer to one) (60) using a four-factor, three-level definitive screening design (3^4) *via* Design Expert® software. The optimum formula involved the following: ratio of PC/PE was at level − 1; ratio of PC + PE/surfactant was at level − 1, type of surfactant was Cremophor RH 40, and type of PE was ethanol. The prepared optimum transferosome was with desirability of 0.752, exhibited entrapment of 72.58 ± 4.51%, *in vitro* release of 79.15 ± 3.72%, and vesicle size of 83.79 ± 3 .1 nm.

The Fourier-transform infrared (FTIR) spectra of pure RES and the physical mixture of the optimized RES-loaded transferosome were compared with and the spectra of each separate component are shown in Fig. 3. There is no shifting observed for peaks relevant to RES and no loss of these peaks, approving that RES stays in its original chemical form within the optimized formula. Also, no extra peaks were observed indicating that loading RES into the transferosomes did not change its nature. Consequently, no physical interaction between RES and transferosome constituents was confirmed, thus RES is compatible with the components of optimized transferosomes (15).

The morphology of optimized RES-loaded transferosome is shown in Fig. 4. The photomicrograph outlines small spherical vesicles with no aggregation and a homogenous size distribution.

Entrapment of the optimized loaded transferosomes and their size were evaluated after 1, 2, and 3 months at 4 and 25°C, as shown in Fig. 5. the result revealed an insignificant decrease in the entrapment, also insignificant increase in transferosomes diameter throughout the 3 months at $P > 0.05$. The increase in transferosomal vesicle size with respect to time had been reported to be due to the tendency of the vesicles to form coalescence as a result of the weak van der Waals and cohesive forces throughout the vesicles (38).

Preparation and Characterization of Mucoadhesive Nasal Gel

The nature of the nasal cavity determines the characteristics required for the mucoadhesive nasal gel, including gelation temperature (should range from 32 to34°C), gelation time (should be short enough to adhere to mucosal membrane to prevent drainage of formula), mucoadhesion strength (should be high enough to increase the residence of the formula in nasal membrane, from 22 to 30 g/cm^2), and gel strength (should range from 25 to 50 s) to maintain the gel integrity for sufficient time (18,61).

Poloxamer 407 (P407) has thermo-reversible properties as a result of its low critical solution temperature; it exhibits a sol–gel transition producing *in situ* gel at body temperature (45). Carbopol is a mucoadhesive and gelling agent, and also it has the ability to enhance the drug's intranasal
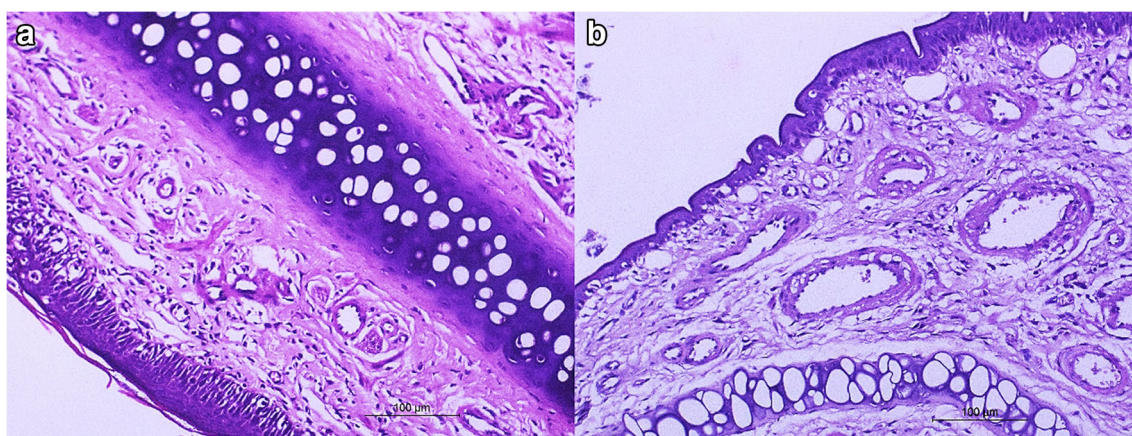
Fig. 9. Light photomicrographs of **a** untreated rat nasal mucosal membrane and **b** rat nasal mucosal membrane treated with RES-trans gel
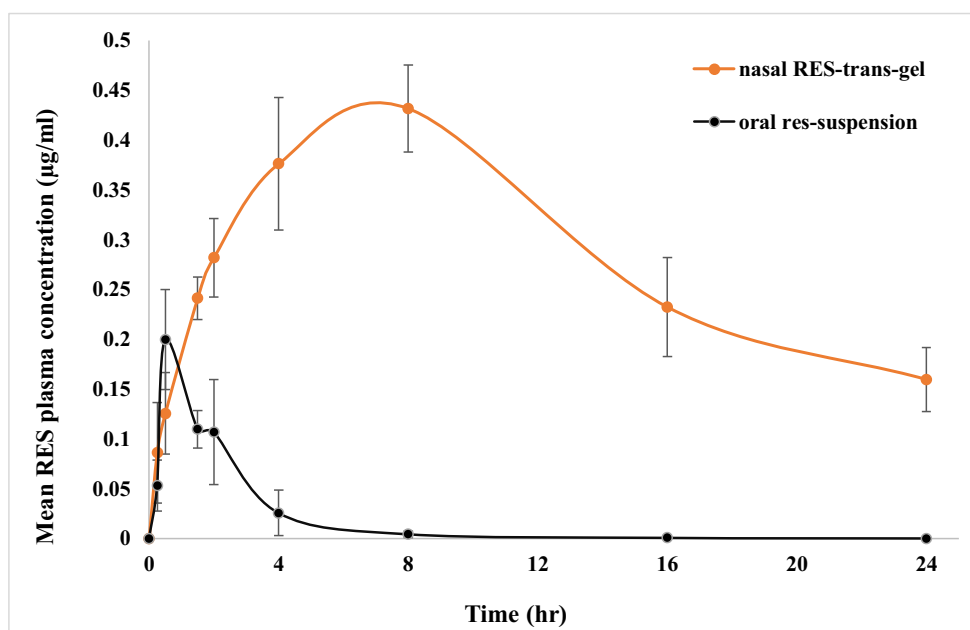
Fig. 10. Mean RES concentrations in plasma of rats after administration of oral RES suspension and intranasal RES-trans gel

bioavailability and increase the stability *via* inhibition of proteolytic enzymes (18,62).

The results revealed that gelation temperature ranged from 21.2 to 45.5°C and gelation time ranged from 14.78 to 55.57 s (Fig. 6). The gelation time and temperature significantly increased with the reduction in poloxamer 407 concentration; no variations were observed upon changing concentration of Carbopol 934 when keeping the concentration of poloxamer 407 constant.

Mucoadhesion strength ranged from 12.16 to 29.03 g/cm^2, while mucoadhesion time ranged from 1.72 to 5.83 h and gel strength ranged from 18.9 to 39.02 s (Fig. 6). The mucoadhesion strength, time, and gel strength significantly increased with increasing poloxamer 407 and especially carbopol concentration (Fig. 6).

Preparation and Characterization of RES-TRS Gel

The FTIR spectra of pure RES and the physical mixture of the optimized RES-trans gel were compared with the spectra of each separate component, as shown in Fig. 3. No peak shifting or peak loss was observed for RES; the result is approving that

Table VII. Pharmacokinetic Parameters for RES in Rat Plasma Following Administration of Oral RES Suspension and Intranasal RES-Trans Gel

Parameters	Oral RES suspension	Nasal RES-trans gel
C_{max} (μg/ml)	0.202 ± 0.05	0.434 ± 0.05
T_{max} (h)	0.75 ± 0.61	7.33 ± 1.63
AUC_{0-24} (μg h/ml)	0.459 ± 0.17	6.847 ± 0.997
$AUC_{0-\infty}$ (μg h/ml)	0.459 ± 0.20	10.335 ± 2.233
$MRT_{0-\infty}$ (h)	2.124 ± 0.53	22.053 ± 5.346
$t_{1/2}$ (h)	2.407 ± 0.99	14.592 ± 3.668

RES stays in its original chemical form within the optimized formula. Also, no extra peaks were observed indicating that incorporating RES-loaded transferosomes into the selected mucoadhesive nasal gel did not change RES nature. Consequently, no physical interaction between RES and the selected gel constituents was confirmed, thus RES is compatible with the components of the selected mucoadhesive nasal gel (15).

The *in vitro* release of RES was significantly higher than the RES suspension and lower than the optimized RES transferosomes (65.87 ± 2.12) (Fig. 7). Presence of carbopol might result in fast dissolution and release while the retardation in the release might be due to presence of poloxamer 407 as a mucoadhesive polymer (63) which was reported to slow down the *in vitro* release of nimesulide (45). The correlation coefficients calculated for *in vitro* release was better described by zero-order model (Table V).

Ex vivo drug permeation study through sheep nasal mucosa showed sustained release of RES for 12 h (Fig. 8), and RES permeation kinetics is shown in Table V. The permeability flux and permeability coefficient for transferosomes were higher than the RES suspension (Table VI). RES-trans gel exhibited a significant increased permeation compared with the RES suspension gel containing an equivalent amount of RES. Several mechanisms have been reported for the enhanced permeation involving presence of Carbopol 934. Carbopol 934 is an anionic polymer that was reported to have a penetration-enhancing effect due to high Ca^{2+} binding capability (63). Also, it had been reported that the enhanced permeation occurs because the loaded vesicle carries the drug throughout the nasal mucosa (64). Another mechanism suggests that the presence of phospholipids increases the affinity of the vesicles for biological membranes, and the flexibility of the transferosomes enables them to squeeze themselves to pass easily through the nasal mucosa (65). Transferosomes were also reported to enhance nasal mucosal permeation by opening new pores through the paracellular tight junctions (66).

Histopathology for Nasal Mucosal Toxicity and Tolerability

The optimized RES-trans gel are composed mainly of phospholipids, surfactants, poloxamer, and carbopol; it is necessary to investigate the safety of these vesicular formulations (67). Photomicrographs taken for nasal mucosa of anterior cross-sections (Fig. 9) show reasonable degenerative changes in olfactory epithelium accompanied by moderate infiltrations of mononuclear cell in the lamina propria, and no signs of severe degenerative changes were observed. Accordingly, histopathology study confirmed the safety of RES-trans gel on sheep nasal mucosa.

In Vivo Pharmacokinetic Study

The RES concentrations in plasma following intranasal administration of the optimized RES-trans gel were found to be significantly higher at all the time points compared to oral RES suspension at $P < 0.05$; the plasma concentration–time profiles are presented in Fig. 10 and Table VII represents the pharmacokinetic parameters of RES.

The obtained results demonstrated that the C_{max} of RES in the optimized RES-trans gel was 2.15 times higher and $AUC_{(0-\infty)}$ was 22.5 times higher than the oral RES suspension. Correspondingly, T_{max} of optimized RES-trans gel increased by 9.7 h compared with oral RES suspension, which is consistent with the differences in RES dissolution enhancement, release retardation, and permeability improvement through the optimized RES-trans gel. The results of the pharmacokinetic parameters were highly significant at $P < 0.05$) for the optimized RES-trans gel compared with oral RES suspension, indicating that the absorption of RES was significantly increased by intranasal transferosome administration. Another *in vivo* pharmacokinetic study by Gurinder and Roopa in male Wistar rats presented enhancement in the oral bioavailability of self-nano-emulsifying drug delivery system by 4.31-fold when compared to that of pure RES (50). Administration of oral RES suspension led to a sharp C_{max} within 0.75 ± 0.61 h then the plasma concentration speedily declined, indicating a rapid metabolism of RES; however, a fairly slow rise was observed which might be explained by the enterohepatic recirculation reported for RES (68). The sustained plasma concentration of RES was obtained up to 24 h after intranasal administration of the optimized RES-trans gel, and the results go with the data obtained for *in vitro* release and *ex vivo* permeation study.

CONCLUSION

In this research, the optimized transferosomes containing Cremophor RH 40, ethanol, and soya lecithin can be well thought out as an efficient nanocarrier for bioavailability enhancement of RES through the nasal route. The optimized transferosomes were found to be safe and tolerable to the sheep nasal mucosa; they displayed vesicle size of 83.79 ± 2.54 nm, entrapment efficiency (EE%) up to $72.58 \pm 4.51\%$, and *ex vivo* permeation up to $75.95 \pm 3.19\%$. The intranasal RES-transferosomal mucoadhesive gel showed gorgeous elevation in $AUC_{(0-\infty)}$ and C_{max} by 22.5 and 2.15 times, respectively, which is counted as a valuable enhancement in the bioavailability of RES compared with oral RES suspension. Therefore, the developed transferosomes could be counted as an elegant nanocarrier for nasal delivery of drugs that have a low oral bioavailability.

REFERENCES

1. Wu CF, Yang JY, Wang F, Wang XX. Resveratrol: botanical origin, pharmacological activity and applications. Chin J Nat Med. 2013;11(1):1–15. https://doi.org/10.1016/S1875-5364(13)60001-1.
2. Jia Y, Liu Z, Huo X, Wang C, Meng Q, Liu Q, et al. Enhancement effect of resveratrol on the intestinal absorption of bestatin by regulating PEPT1, MDR1 and MRP2 in vivo and in vitro. Int J Pharm. 2015;495(1):588–98. https://doi.org/10.1016/j.ijpharm.2015.09.042.
3. Shi G, Rao L, Yu H, Xiang H, Yang H, Ji R. Stabilization and encapsulation of photosensitive resveratrol within yeast cell. Int J Pharm. 2008;349(1–2):83–93.
4. Park SN, Jo NR, Jeon SH. Chitosan-coated liposomes for enhanced skin permeation of resveratrol. J Ind Eng Chem. 2014;20(4):1481–5. https://doi.org/10.1016/j.jiec.2013.07.035.
5. Anekonda TS. Resveratrol—a boon for treating Alzheimer's disease? Brain Res Rev. 2006;52:316–26.
6. Wang H, Jiang T, Li W, Gao N, Zhang T. Resveratrol attenuates oxidative damage through activating mitophagy in an in vitro model of Alzheimer's disease. Toxicol Lett. 2018;282:100–8. https://doi.org/10.1016/j.toxlet.2017.10.021.
7. Amri A, Chaumeil JC, Sfar S, Charrueau C. Administration of resveratrol: what formulation solutions to bioavailability limitations? J Control Release. 2012;158(2):182–93. https://doi.org/10.1016/j.jconrel.2011.09.083.
8. Summerlin N, Soo E, Thakur S, Qu Z, Jambhrunkar S, Popat A. Resveratrol nanoformulations: challenges and opportunities. Int J Pharm. 2015;479(2):282–90. https://doi.org/10.1016/j.ijpharm.2015.01.003.
9. Summerlin N, Qu Z, Pujara N, Sheng Y, Jambhrunkar S, McGuckin M, et al. Colloidal mesoporous silica nanoparticles enhance the biological activity of resveratrol. Colloids Surfaces B Biointerfaces. 2016;144:1–7. https://doi.org/10.1016/j.colsurfb.2016.03.076.
10. Venuti V, Cannavà C, Cristiano MC, Fresta M, Majolino D, Paolino D, et al. A characterization study of resveratrol/sulfobutyl ether-β-cyclodextrin inclusion complex and in vitro anticancer activity. Colloids Surf B Biointerfaces. 2014;115:22–8.
11. Lu X, Ji C, Xu H, Li X, Ding H, Ye M, et al. Resveratrol-loaded polymeric micelles protect cells from Aβ-induced oxidative stress. Int J Pharm. 2009;375(1–2):89–96.
12. Ota A, Djordjevi VB, Sentjurc M, Balanč BD, Ota A, Djordjević VB, et al. Resveratrol-loaded liposomes: interaction of resveratrol with phospholipids. Eur J Lipid Sci Technol. 2015;117:1615–26.

13. Scalia S, Trotta V, Iannuccelli V, Bianchi A. Enhancement of in vivo human skin penetration of resveratrol by chitosan-coated lipid microparticles. Colloids Surfaces B Biointerfaces. 2015;135:42–9. https://doi.org/10.1016/j.colsurfb.2015.07.043.

14. Friedrich RB, Kann B, Coradini K, Offerhaus HL, Beck RCR, Windbergs M. Skin penetration behavior of lipid-core nanocapsules for simultaneous delivery of resveratrol and curcumin. Eur J Pharm Sci. 2015;78:204–13. https://doi.org/10.1016/j.ejps.2015.07.018.

15. Ramalingam P, Ko YT. Improved oral delivery of resveratrol from N-trimethyl chitosan-g-palmitic acid surface-modified solid lipid nanoparticles. Colloids Surfaces B Biointerfaces. 2016;139:52–61. https://doi.org/10.1016/j.colsurfb.2015.11.050.

16. Hung C-F, Chen J-K, Liao M-H, Lo H-M, Fang J-Y. Development and evaluation of emulsion-liposome blends for resveratrol delivery. J Nanosci Nanotechnol. 2006;6(9):2950–8.

17. Press D. Development , characterization , and skin delivery studies of related ultradeformable vesicles: transfersomes, ethosomes, and transethosomes. Int J Nanomedicine. 2015;18(10):5837–51.

18. Mura P, Mennini N, Nativi C, Richichi B. In situ mucoadhesive-thermosensitive liposomal gel as a novel vehicle for nasal extended delivery of opiorphin. Eur J Pharm Biopharm. 2018;122:54–61. https://doi.org/10.1016/j.ejpb.2017.10.008.

19. Sonvico F, Clementino A, Buttini F, Colombo G, Pescina S, Guterres SS, et al. Surface-modified nanocarriers for nose-to-brain delivery: from bioadhesion to targeting. Pharmaceutics. 2018;10(1):1–33.

20. Bernkop-schn A. Nasal drug delivery: design of a novel mucoadhesive and in situ gelling polymer. Int J Pharm. 2017;517(1–2):196–202. https://doi.org/10.1016/j.ijpharm.2016.11.055.

21. Bitter C, Suter-Zimmermann K, Surber C. Nasal drug delivery in humans. Curr Probl Dermatol. 2011;40:20–35. https://doi.org/10.1159/000321044.

22. Pardeshi CV, Belgamwar VS. Direct nose to brain drug delivery via integrated nerve pathways bypassing the blood–brain barrier: an excellent platform for brain targeting. Expert Opin Drug Deliv. 2013;10(7):957–72.

23. Espinoza LC, Vacacela M, Clares B, Garcia ML, Fabrega MJCA. Development of a nasal donepezil-loaded microemulsion for the treatment of Alzheimer's disease: in vitro and ex vivo characterization. CNS Neurol Disord Drug Targets. 2018;17(1):43–53.

24. Gartziandia O, Herrán E, Ruiz-Ortega JA, Miguelez C, Igartua M, Lafuente JV, et al. Intranasal administration of chitosan-coated nanostructured lipid carriers loaded with GDNF improves behavioral and histological recovery in a partial lesion model of Parkinson's disease. J Biomed Nanotechnol. 2016;12(12):2220–30.

25. Wang Y, Li M, Qian S, Zhang Q, Zhou L, Zuo Z, et al. Zolpidem mucoadhesive formulations for intranasal delivery: characterization, in vitro permeability, pharmacokinetics, and nasal ciliotoxicity in rats. J Pharm Sci. 2016;105(9):2840–7.

26. Piazza J, Hoare T, Molinaro L, Terpstra K, Bhandari J, Selvaganapathy PR, et al. Haloperidol-loaded intranasally administered lectin functionalized poly(ethylene glycol)-block-poly(D,L)-lactic-co-glycolic acid (PEG-PLGA) nanoparticles for the treatment of schizophrenia. Eur J Pharm Biopharm. 2014;87(1):30–9. https://doi.org/10.1016/j.ejpb.2014.02.007.

27. Chaurasia S, Dogra SS, EUROPEAN JOURNAL OF EJPMR TRANSFERSOMES. Novel approach for intranasal delivery. Eur J Pharm Med Res. 2017;4(3):192–203.

28. Karavasili C, Fatouros DG. Smart materials: in situ gel-forming systems for nasal delivery. Drug Discov Today. 2015;21(1):157–66. https://doi.org/10.1016/j.drudis.2015.10.016.

29. Cevc G, Blume G. Lipid vesicles penetrate into intact skin owing to the transdermal osmotic gradients and hydration force. BBA - Biomembr. 1992;1104(1):226–32.

30. Aboud HM, Ali AA, El-menshawe SF, Elbary AA. Nanotransfersomes of carvedilol for intranasal delivery: formulation, characterization and in vivo evaluation. Drug Deliv. 2016;23(7):2471–81. https://doi.org/10.3109/10717544.2015.1013587.

31. Ghanbarzadeh S, Arami S. Formulation and evaluation of piroxicam transferosomal gel: an approach for penetration enhancement. J Drug Deliv Sci Technol. 2013;23(6):587–90. https://doi.org/10.1016/S1773-2247(13)50089-X.

32. Malakar J, Oomen S, Nayak AK. Formulation, optimization and evaluation of transferosomal gel for transdermal insulin delivery. Saudi Pharm J. 2012;20(4):355–63. https://doi.org/10.1016/j.jsps.2012.02.001.

33. Ahmed H, Shuwaili AL, Bazigha K, Abdul Rasool AAA. Optimization of elastic transfersomes formulations for transdermal delivery of pentoxifylline. Eur J Pharm Biopharm. 2016;102:101–14. https://doi.org/10.1016/j.ejpb.2016.02.013.

34. Callens C, Ceulemans J, Ludwig A, Foreman P, Remon JP. Rheological study on mucoadhesivity of some nasal powder formulations. Eur J Pharm Biopharm. 2003;55:323–8.

35. Chaudhary H, Kohli K, Kumar V. Nano-transfersomes as a novel carrier for transdermal delivery. Int J Pharm. 2013;454(1):367–80. https://doi.org/10.1016/j.ijpharm.2013.07.031.

36. Salem HF, Ahmed SM, Hassaballah AE, Omar MM. Targeting brain cells with glutathione-modulated nanoliposomes: in vitro and in vivo study. Drug Des Devel Ther. 2015;9:3705–27.

37. Jose S, Anju SS, Cinu TA, Aleykutty NA, Thomas S, Souto EB. In vivo pharmacokinetics and biodistribution of resveratrol-loaded solid lipid nanoparticles for brain delivery. Int J Pharm. 2014;474(1–2):6–13. https://doi.org/10.1016/j.ijpharm.2014.08.003.

38. Salem HF, Kharshoum RM, El-ela FIA, F AG, Abdellatif KRA. Evaluation and optimization of pH-responsive niosomes as a carrier for efficient treatment of breast cancer. Drug Deliv Transl Res. 2018;8(3):633–44.

39. Salem HF, Ahmed SM, Omar MM. Liposomal flucytosine capped with gold nanoparticle formulations for improved ocular delivery. Drug Des Devel Ther. 2016;10:277–95.

40. Shamma RN, Elsayed I. Transfersomal lyophilized gel of buspirone HCl: formulation, evaluation and statistical optimization. J Liposome Res. 2013;23(3):244–54.

41. Ammar HO, Haider M, Ibrahim M, El Hoffy NM. In vitro and in vivo investigation for optimization of niosomal ability for sustainment and bioavailability enhancement of diltiazem after nasal administration. Drug Deliv. 2017;24(1):414–21.

42. Gupta V, Trivedi P. Enhancement of storage stability of cisplatin-loaded protransfersome topical drug delivery system by surface modification with block copolymer and gelling agent. J Drug Deliv Sci Technol. 2012;22(4):361–6. https://doi.org/10.1016/S1773-2247(12)50060-2.

43. Shelke S, Shahi S, Jadhav K, Dhamecha D, Tiwari R, Patil H. Thermoreversible nanoethosomal gel for the intranasal delivery of eletriptan hydrobromide. J Mater Sci Mater Med. 2016;27(6):1–13.

44. Moawad FA, Ali AA & Salem HF. Nanotransfersomes-loaded thermosensitive in situ gel as a rectal delivery system of tizanidine HCl: preparation, in vitro and in vivo performance. Drug Delivery. 2017;24:1, 252–260.

45. Yuan Y, Cui Y, Zhang L, Zhu HP, Guo YS, Zhong B, et al. Thermosensitive and mucoadhesive in situ gel based on poloxamer as new carrier for rectal administration of nimesulide. Int J Pharm. 2012;430(1–2):114–9. https://doi.org/10.1016/j.ijpharm.2012.03.054.

46. Elkomy MH, El-menshawe SF, Ali AA, Halawa AA, El-din ASGS. Betahistine dihydrochloride transdermal delivery via optimized thermosensitive gels: percutaneous absorption evaluation using rat growth as a biomarker. Drug Deliv Transl Res. 2017;8(1):165–77.

47. Rajput A, Bariya A, Allam A, Othman S, Butani SB. In situ nanostructured hydrogel of resveratrol for brain targeting: in vitro–in vivo characterization. Drug Deliv Transl Res. 2018;8(5):1460–70.

48. Basu S, Maity S. Preparation and characterisation of mucoadhesive nasal gel of venlafaxine hydrochloride for treatment of anxiety disorders. Indian J Pharm Sci. 2012;74(5):428–33.

49. Cao S, Ren X, Zhang Q, Chen E, Xu F, Chen J, et al. In situ gel based on gellan gum as new carrier for nasal administration of mometasone furoate. Int J Pharm. 2009;365:109–15.

50. Singh G, Pai RS. Trans-Resveratrol self-nano-emulsifying drug delivery system (SNEDDS) with enhanced bioavailability potential: optimization, pharmacokinetics and in situ single pass intestinal perfusion (SPIP) studies. Drug Deliv. 2014;22(4):522–30.

51. Hao J, Zhao J, Zhang S, Tong T, Zhuang Q, Jin K, et al. Fabrication of an ionic-sensitive in situ gel loaded with resveratrol nanosuspensions intended for direct nose-to-brain delivery. Colloids Surfaces B Biointerfaces. 2016;147:376–86. https://doi.org/10.1016/j.colsurfb.2016.08.011.

52. Singh G, Pai RS, Pandit V. In vivo pharmacokinetic applicability of a simple and validated HPLC method for orally administered trans-resveratrol loaded polymeric nanoparticles to rats. J Pharm Investig. 2014;44(2):69–78.

53. Taher M, Mahmood S, Taher M, Mandal UK. Experimental design and optimization of raloxifene hydrochloride loaded nanotransfersomes for transdermal application. Int J Nanomedicine. 2014;9:4331–46.

54. Basavaraj S, Betageri GV. Improved oral delivery of resveratrol using proliposomal formulation: investigation of various factors contributing to prolonged absorption of unmetabolized resveratrol. Expert Opin Drug Deliv. 2014;11(4):493–503.

55. Duangjit S, Opanasopit P, Rojanarata T, Characterization NT. In vitro skin permeation of meloxicam-loaded liposomes versus transfersomes. J Drug Deliv. 2011;2011:1–9.

56. Al-Mahallawi AM, Khowessah OM, Shoukri RA. Nano-transfersomal ciprofloxacin loaded vesicles for non-invasive trans-tympanic ototopical delivery: in-vitro optimization, ex-vivo permeation studies, and in-vivo assessment. Int J Pharm. 2014;472(1–2):304–14. https://doi.org/10.1016/j.ijpharm.2014.06.041.

57. Karim NA. Ethosomal nanocarriers: the impact of constituents and formulation techniques on ethosomal properties, in vivo studies, and clinical trials. Int J Nanomedicine. 2016;11:2279–304.

58. El-Menshawe SF, Ali AA, Halawa AA, Srag El-din ASG. A novel transdermal nanoethosomal gel of betahistine dihydrochloride for weight gain control: in-vitro and in-vivo characterization. Drug Des Devel Ther. 2017;11:3377–88.

59. Manconi M, Caddeo C, Sinico C, Valenti D, Cristina M, Biggio G, et al. Ex vivo skin delivery of diclofenac by transcutol containing liposomes and suggested mechanism of vesicle–skin interaction. Eur J Pharm Biopharm. 2011;78(1):27–35. https://doi.org/10.1016/j.ejpb.2010.12.010.

60. Das SK, Yuvaraja K, Khanam J, Nanda A. Formulation development and statistical optimization of ibuprofen-loaded polymethacrylate microspheres using response surface methodology. Chem Eng Res Des. 2015;96:1–14. https://doi.org/10.1016/j.cherd.2015.01.014.

61. Xu X, Shen Y, Wang W, Sun C, Li C, Xiong Y, et al. Preparation and in vitro characterization of thermosensitive and mucoadhesive hydrogels for nasal delivery of phenylephrine hydrochloride. Eur J Pharm Biopharm. 2014;88(3):998–1004. https://doi.org/10.1016/j.ejpb.2014.08.015.

62. Ahad A, Al-saleh AA, Al-mohizea AM, Al-jenoobi FI, Raish M, Eldeen A, et al. Pharmacodynamic study of eprosartan mesylate-loaded transfersomes Carbopol 1 gel under Dermaroller 1 on rats with methyl prednisolone acetate-induced hypertension. Biomed Pharmacother. 2017;89:177–84. https://doi.org/10.1016/j.biopha.2017.01.164.

63. Majithiya RJ, Ghosh PK, Umrethia ML, Murthy RSR. Thermoreversible-mucoadhesive gel for nasal delivery of suma-triptan. AAPS PharmSciTech. 2006;7(3):1–7.

64. Cevc G, Blume G. Hydrocortisone and dexamethasone in very deformable drug carriers have increased biological potency, prolonged effect, and reduced therapeutic dosage. Biochim Biophys Acta. 2004;1663(1–2):61–73.

65. Ahad A, Aqil M, Kohli K, Sultana Y, Mujeeb M, Ali A. Formulation and optimization of nanotransfersomes using experimental design technique for accentuated transdermal delivery of valsartan. Nanomedicine. 2012;8(2):237–49.

66. Mara Mainardes R, Cristina Cocenza Urban M, Oliveira Cinto P, Vinicius Chaud M, Cesar Evangelista R, PDGM. Liposomes and micro/nanoparticles as colloidal carriers for nasal drug delivery. Curr Drug Deliv. 2006;3(3):275–85.

67. Salunke SR, Patil SB. Ion activated in situ gel of gellan gum containing salbutamol sulphate for nasal administration. Int J Biol Macromol. 2016;87:41–7. https://doi.org/10.1016/j.ijbiomac.2016.02.044.

68. Singh G, Pai RS. Recent advances of resveratrol in nanostructured based delivery systems and in the management of HIV/AIDS. J Control Release. 2014;194:178–88. https://doi.org/10.1016/j.jconrel.2014.09.002.